

pubs.acs.org/JPCA Article

Detangling Solvatochromic Effects by the Effective Fragment Potential Method

Published as part of The Journal of Physical Chemistry A virtual special issue "Krishnan Raghavachari Festschrift".

Lyudmila V. Slipchenko*



Cite This: J. Phys. Chem. A 2024, 128, 656-669



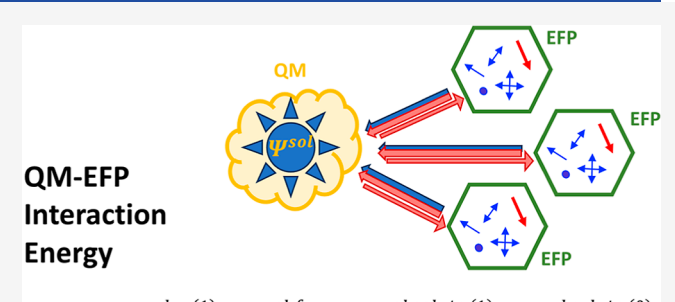
ACCESS

Metrics & More

Article Recommendations

SI Supporting Information

ABSTRACT: Understanding molecular interactions in complex systems opens avenues for the efficient design of new materials with target properties. Energy decomposition methods provide a means to obtain a detailed picture of intermolecular interactions. This work introduces a molecular modeling approach for decomposing the solvatochromic shifts of the electronic excited states into the contributions of the individual molecular fragments of the environment surrounding the chromophore. The developed approach is implemented for the QM/EFP (quantum mechanics/effective fragment potential) model that provides a rigorous first-principles-based description of the electronic states of the chromophores in complex polarizable environments. On the



 $E_{QM-EFP} = E^{elec\,(1)} + E^{pol\,frag} + E^{pol\,solute\,(1)} + E^{pol\,solute\,(0)}$

example of two model systems, water pentamer and hydrated uracil, we show how the decomposition of the solvatochromic shifts into the contributions of individual solvent water molecules provides a detailed picture of the intermolecular interactions in the ground and excited states of these systems. The analysis also demonstrates the nonadditivity of solute—solvent interactions and the significant contribution of solute polarization to the total values of solvatochromic shifts.

■ INTRODUCTION

A strength of atomistic molecular modeling is its ability to provide mechanistic details about the system interactions. However, while the wave function contains all information about the system, specific analysis tools are needed for extracting such information. For example, in studies of ligand-protein binding energies, structure-function relations can be obtained from a map of pairwise interactions between the ligand and protein components. Such interaction maps not only provide insight into molecular-level interactions in the system but also can guide function optimizations by mutagenesis. In recent years, several computational tools for decomposing the total system energy into pairwise contributions have been developed, including pairwise interaction energy decomposition analysis (PIEDA) extension of the fragment molecular orbital (FMO) method, and functional symmetry-adapted perturbation theory (F-SAPT).¹⁻⁵ Similar questions about structure-function relations in extended photochemically active systems might be even more acute. For example, while mutagenesis is an established technique for elucidating details of light-induced processes in photosynthetic pigment-protein complexes and proteins of the GFP family, theoretical tools for the analysis of mutagenesis's effects on proteins' photochemistry still need to be developed. 6-11 Additionally, as electronically excited states

are often delocalized, the results of mutagenesis on the photochemical processes might be more convoluted and less linear than in the case of the ground state. In this article, we address the question of structure-function relations in extended photoactive systems by introducing a new computational technique for the pairwise decomposition analysis of solvatochromic shifts in embedded electronically excited chromophores. By analogy to the interaction maps for ligand-protein binding, pairwise maps of solvatochromic shifts facilitate a molecular-level understanding and control of the optical properties of photoactive systems. The pairwise excitation energy decomposition analysis (PEEDA) developed in this work is complementary to the existing tools for the analysis of electronic states, such as the decomposition of excitation energies into physically meaningful Coulomb and exchange components, 12 the multistate decomposition of energies in excimers, 13 and the analysis of excitonically coupled systems in

Received: September 14, 2023 Revised: December 22, 2023 Accepted: December 23, 2023 Published: January 9, 2024





terms of one-body and two-body contributions. ^{14,15} PEEDA provides a currently missing link in our understanding of excitation energies in complex systems, namely, how the solvent-induced shift to the excited state is distributed into the contributions of individual solvent molecules or fragments.

The PEEDA introduced in this work is developed for the polarizable embedding quantum mechanics/effective fragment potential (QM/EFP) models. ^{16–21} EFP is a polarizable model for describing noncovalent interactions. ^{21–25} EFP represents a molecular system as a combination of fragments interacting through electrostatic, polarization, dispersion, exchange-repulsion, and optional charge-transfer terms. Each energy term is derived from the perturbation theory applied to a noninteracting system, with the long-range expansion in the orders of the Coulomb operator resulting in electrostatic, polarization, and dispersion terms and the short-range expansion in the powers of intermolecular overlap responsible for exchange-repulsion and charge-transfer terms. EFP is similar in spirit to the symmetryadapted perturbation theory (SAPT)^{26,27} that also utilizes perturbation theory to describe noncovalent interactions between the fragments. However, unlike SAPT, in which the system is described fully quantum-mechanically, each fragment in EFP is represented by a set of precomputed parameters (distributed electrostatic multipoles, static and dynamic polarizabilities, localized wave function, etc.). This parameterization dramatically decreases the computational cost of EFP and makes it suitable for simulating systems containing thousands of fragments. When combined with a QM region, EFP provides a polarizable embedding in which electron distribution in the quantum and EFP subsystems (represented by induced dipoles) is solved self-consistently. Recently, we extended the QM/EFP models to full embedding schemes, in which the short-range dispersion and exchange-repulsion terms additionally couple QM and EFP regions. $^{28-30}$ We also demonstrated that the inclusion of the exchange-repulsion term in QM/EFP systematically improves the description of electronic states with a partial charge transfer from solvent to solute, which is typical for n-pi* excitations in chromophores with strong H-bonds to solvent molecules.³⁰ Recently, the EFP and QM/EFP models were extended to biological polymers and macromolecules.³¹ In the original formulation of EFP, effective fragments were rigid molecules, which limited the method to solvents without torsional flexibility, such as water or benzene. We designed a procedure for splitting a macromolecule into effective fragments and allowing the fragments to acquire different geometries ("flexible fragments") without losing accuracy and computational cost.³² These developments make QM/EFP a reliable method for modeling photo- and redox-active chemistry in proteins and synthetic polymers. 10,33,34

In this work, we develop a computational approach in which QM/EFP solvatochromic shifts of electronically excited states of solvated chromophores are decomposed into contributions of individual solvent fragments (generally, here and later, "solvent" is used to refer to a chromophore environment). Such a decomposition is conducted in a polarized system and implicitly incorporates many-body effects. While PEEDA is implemented in the framework of QM/EFP, it can be extended to other embedded models for electronically excited states, including electrostatic embedding QM/MM and frozen embedding DFT methods. 35,36

METHODS

QM/EFP PEEDA is motivated by two models: the EFP pairwise energy analysis recently introduced in ref 32 and the decomposition of QM/EFP solvatochromic shifts into principle components (electrostatic, solute- and solvent-induced polarization, and remainder terms) developed by DeFusco et al. in the context of the state-averaged CASSCF/EFP1 model. We briefly summarize both approaches to bring PEEDA into context.

EFP Pairwise Energy Analysis. The EFP noncovalent interaction energy $E_{EFP-EFP}$ consists of electrostatic (E^{elec}), polarization or induction (E^{pol}), dispersion (E^{disp}), and exchange-repulsion ($E^{\mathrm{ex-rep}}$) contributions

$$E_{\rm EFP-EFP} = E_{\rm EFP}^{\rm elec} + E_{\rm EFP}^{\rm pol} + E_{\rm EFP}^{\rm disp} + E_{\rm EFP}^{\rm ex-rep} \tag{1}$$

While the charge-transfer energy can be significant in ionic systems, 17,38,39 it is typically the smallest by magnitude energy term in neutral systems and is not considered in this work. In the EFP pairwise energy decomposition analysis, 32 the system interaction energy $E_{\rm EFP-EFP}$ is split into the contributions of each pair of fragments. Electrostatic, dispersion, and exchange-repulsion terms are modeled as two-body interactions, so pairwise fragment—fragment interactions sum into the corresponding system energies. The pairwise decomposition of the many-body polarization energy is computed for the self-consistently converged fragments' induced dipoles. For example, the pairwise polarization contribution for a pair of fragments A and B is

$$E_{\rm EFP}^{\rm pol,AB} = -\frac{1}{2} \sum_{a}^{x,y,z} \left[\sum_{p \in A} \mu_a^p F_a^{B,p} + \sum_{p \in B} \mu_a^p F_a^{A,p} \right] \tag{2}$$

where μ_a^p is the ath Cartesian component of the induced dipole moment at the polarizability point p (belonging either to fragment A or B) and $F_a^{\mathrm{B}/\mathrm{A},p}$ is the ath Cartesian component of the electric field at point p due to all nuclei and static multipoles of fragment B or A. In this formulation, the total polarization energy is the sum of all pairwise energies. Still, each dimer energy implicitly incorporates many-body effects through the induced dipoles, which are self-consistently converged for the whole system. Thus, the pairwise EFP scheme can provide an interaction map of the entire system or characterize the interactions of a particular fragment with other fragments.

QM/EFP Energy Decomposition. In polarizable embedding, the total QM/EFP energy of the ground state is

$$\begin{split} E_{\text{QM/EFP,gr}} &= \langle \Psi_{\text{gr}}^{\text{sol}} | \hat{H}_{\text{QM}} + \hat{V}^{\text{coul}} + \hat{V}_{\text{gr}}^{\text{pol}} | \Psi_{\text{gr}}^{\text{sol}} \rangle \\ &+ E_{\text{QMnuc-EFP}}^{\text{coul}} + E_{\text{gr}}^{\text{pol}} + E_{\text{QM-EFP}}^{\text{disp}} \\ &+ E_{\text{QM-EFP}}^{\text{covel}} + E_{\text{EFP}}^{\text{coul}} \end{split}$$

$$+ E_{\text{EFP}}^{\text{disp}} + E_{\text{EFP}}^{\text{ex-rep}} \tag{3}$$

where $\Psi^{\rm sol}_{\rm gr}$ is the electronic wave function of the ground state of the solvated system and $\hat{H}_{\rm QM}$ is the molecular Hamiltonian of the quantum subsystem. Dispersion and exchange-repulsion interactions between QM and EFP subsystems ($E^{\rm disp}_{\rm QM-EFP}$ and $E^{\rm ex-rep}_{\rm QM-EFP}$, respectively) are considered here at the EFP level by representing the quantum region with dispersion and exchange-repulsion EFP parameters. A quantum-mechanical treatment of these terms, corresponding to a full embedding model, is described in refs 28–30. $E^{\rm coul}_{\rm QMnuc-EFP}$ is a Coulomb interaction

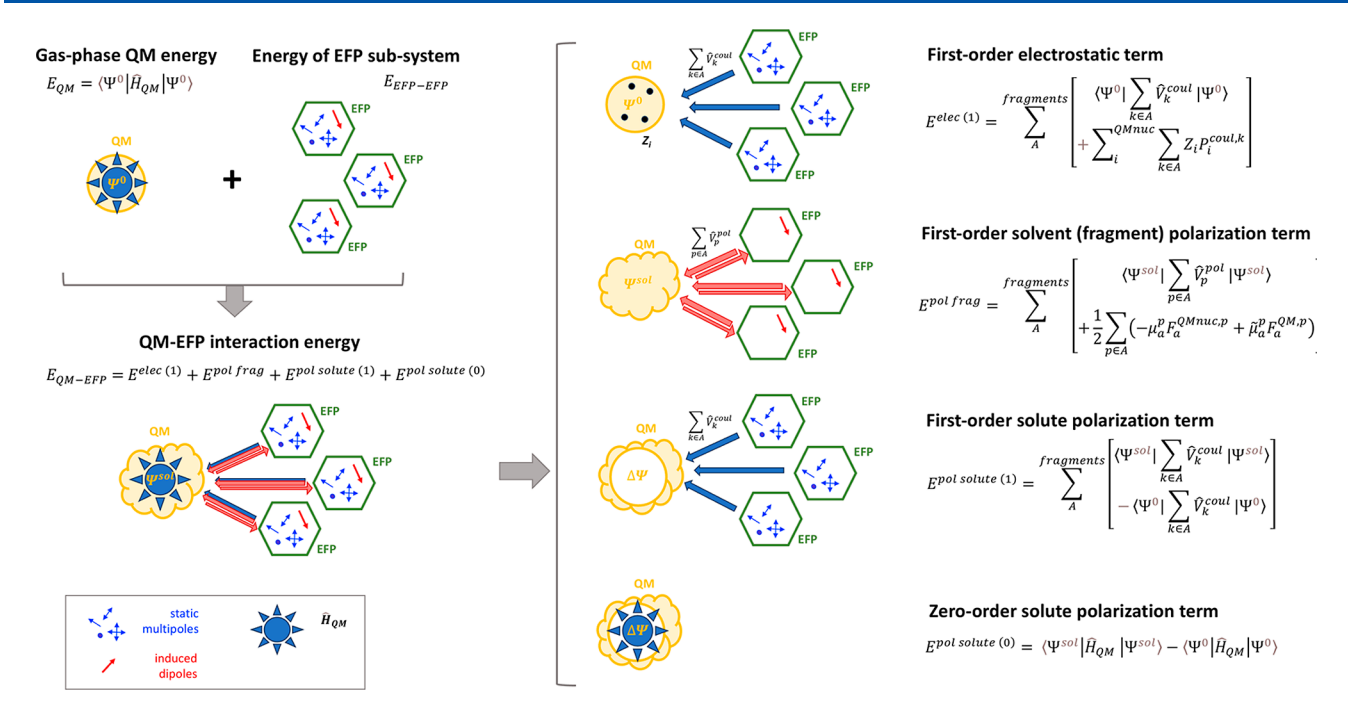


Figure 1. Principal scheme of QM/EFP PEEDA.

energy between the nuclei of the QM region and EFP multipoles.

The Coulomb one-electron operator \hat{V}^{coul} is a sum of contributions due to fragment multipole expansion points k

$$\hat{V}^{\text{coul}} = \sum_{k} \hat{V}_{k}^{\text{coul}}$$

$$V_{k}^{\text{coul}}(x) = q^{k} T(r_{kx}) - \sum_{a}^{x,y,z} \mu_{a}^{k} T_{a}(r_{kx}) + \frac{1}{3} \sum_{a,b}^{x,y,z} \Theta_{ab}^{k} T_{ab}(r_{kx})$$

$$- \frac{1}{15} \sum_{a,b,c}^{x,y,z} \Omega_{abc}^{k} T_{abc}(r_{kx})$$
(4)

where q, μ , Θ , and Ω are the charge, dipole, quadrupole, and octopole moments at the fragment multipole expansion point k. T, T_{ab} , and T_{abc} are the electrostatic tensors of ranks zero to three. The distance between the expansion point k and the coordinate of an electron x in the QM region is denoted as r_{kx} . Similarly, the polarization one-electron operator $\hat{V}_{\rm gr}^{\rm pol} = \sum_{p} \hat{V}_{\rm gr,p}^{\rm pol}$ is

$$V_{\text{gr},p}^{\text{pol}}(x) = -\frac{1}{2} \sum_{a}^{x,y,z} (\mu_a^p + \tilde{\mu}_a^p) T_a(r_{px})$$
(5)

The subscript "gr" denotes that the EFP polarization is self-consistent with the ground-state QM wave function. Induced dipoles μ and conjugated induced dipoles $\tilde{\mu}$ are positioned at the localized molecular orbital centroids (points p in eq 5 and below) of EFP fragments.

Polarization energy $E_{\rm gr}^{\rm pol}$ in eq 3 includes interactions among the effective fragments (the first term in eq 6) and the contribution to the QM–EFP polarization energy (the two terms in square brackets)

$$E_{gr}^{pol} = \frac{1}{2} \sum_{a}^{x,y,z} \sum_{p} \left(-\mu_{a}^{p} F_{a}^{\text{mult},p} + \left[-\mu_{a}^{p} F_{a}^{\text{QMnuc},p} + \tilde{\mu}_{a}^{p} F_{a}^{\text{QM,p}} \right] \right)$$

$$(6)$$

 $F^{\mathrm{mult},p}$ is the electric field at the polarization point p due to the multipole moments of the other effective fragments; $F^{\mathrm{QMnuc},p}$ and $F^{\mathrm{QM},p}$ are the nuclear and electronic fields of the QM region, respectively. Effectively, polarization interactions between the QM and EFP subsystems are separated into two terms, one coming from eq 5, corresponding to the interaction of the QM electron density with the field of fragments' induced dipoles, and the second arising from eq 6, in which the fields of the QM nuclei and electrons interact with the fragments' induced dipoles.

In ref 37, DeFusco et al. developed a decomposition of the total QM-EFP energy (in the context of the EFP1 water model) into contributions from electrostatic, solute and solvent polarization, and remainder EFP terms. EFP1 is an EFP-based water model in which the exchange-repulsion and charge-transfer contributions are modeled with a remainder term fitted to the HF or DFT energies of water dimers and trimers. ^{23,40} The QM/EFP1 energy of the molecular system in the ground electronic state is given by

$$\begin{split} E_{\rm QM/EFP1} &= \langle \Psi_{\rm gr}^{\rm sol} | \hat{H}_{\rm QM} + \hat{V}^{\rm coul} + \hat{V}_{\rm gr}^{\rm pol} + \hat{V}^{\rm rem} | \Psi_{\rm gr}^{\rm sol} \rangle \\ &+ E_{\rm gr}^{\rm pol} + E_{\rm EFP}^{\rm coul} + E_{\rm EFP}^{\rm rem} \end{split} \tag{7}$$

where $E_{\rm EFP}^{\rm rem}$ and $\hat{V}^{\rm rem}$ are the remainder EFP–EFP energy and QM–EFP one-electron potential, respectively, that account for exchange-repulsion, charge-transfer, and higher-order interaction terms.

The QM/EFP1 energy decomposition distinguishes the following contributions³⁷

$$\begin{split} E_{\rm QM/EFP1} &= \langle \Psi_{\rm gr}^{0} | \hat{H}_{\rm QM} | \Psi_{\rm gr}^{0} \rangle + \langle \Psi_{\rm gr}^{0} | \hat{V}^{\rm coul} | \Psi_{\rm gr}^{0} \rangle \\ &+ \langle \Psi_{\rm gr}^{0} | \hat{V}^{\rm rem} | \Psi_{\rm gr}^{0} \rangle + \end{split}$$

$$\begin{split} [\langle \Psi_{\text{gr}}^{\text{sol}} | \hat{H}_{\text{QM}} | \Psi_{\text{gr}}^{\text{sol}} \rangle &- \langle \Psi_{\text{gr}}^{0} | \hat{H}_{\text{QM}} | \Psi_{\text{gr}}^{0} \rangle] \\ &+ [\langle \Psi_{\text{gr}}^{\text{sol}} | \hat{V}^{\text{coul}} + \hat{V}^{\text{rem}} | \Psi_{\text{gr}}^{\text{sol}} \rangle \\ &- \langle \Psi_{\text{gr}}^{0} | \hat{V}^{\text{coul}} + \hat{V}^{\text{rem}} | \Psi_{\text{gr}}^{0} \rangle] + \end{split}$$

$$\left[\left\langle \Psi_{\rm gr}^{\rm sol} | \hat{V}_{\rm gr}^{\rm pol} | \Psi_{\rm gr}^{\rm sol} \right\rangle + E_{\rm gr}^{\rm pol}\right] + \left[E_{\rm EFP}^{\rm coul} + E_{\rm EFP}^{\rm rem}\right] \tag{8}$$

The meaning of different terms in eq 8 is provided below. The solute energy $E_{\rm QM,gr}$ is

$$E_{\rm QM,gr} = \langle \Psi_{\rm gr}^0 | \hat{H}_{\rm QM} | \Psi_{\rm gr}^0 \rangle \tag{9}$$

where Ψ^0_{gr} is the gas-phase ground-state wave function. The first-order solute—solvent electrostatic and remainder energies are

$$E^{\text{elec}(1)} = \langle \Psi_{\text{gr}}^{0} | \hat{V}^{\text{coul}} | \Psi_{\text{gr}}^{0} \rangle \tag{10}$$

$$E^{\text{rem}(1)} = \langle \Psi_{\text{gr}}^{0} | \hat{V}^{\text{rem}} | \Psi_{\text{gr}}^{0} \rangle \tag{11}$$

The solute induction (polarization) energy of the zero and first orders is

$$\begin{split} E^{\text{pol solute}} &= E^{\text{pol solute}(0)} + E^{\text{pol solute}(1)} \\ &= [\langle \Psi_{\text{gr}}^{\text{sol}} | \hat{H}_{\text{QM}} | \Psi_{\text{gr}}^{\text{sol}} \rangle - \langle \Psi_{\text{gr}}^{0} | \hat{H}_{\text{QM}} | \Psi_{\text{gr}}^{0} \rangle] + \\ [\langle \Psi_{\text{gr}}^{\text{sol}} | \hat{V}^{\text{coul}} + \hat{V}^{\text{rem}} | \Psi_{\text{gr}}^{\text{sol}} \rangle - \langle \Psi_{\text{gr}}^{0} | \hat{V}^{\text{coul}} + \hat{V}^{\text{rem}} | \Psi_{\text{gr}}^{0} \rangle] \end{split}$$

$$(12)$$

The fragment induction (polarization) energy is

$$E^{\text{pol frag}} = \langle \Psi_{\text{gr}}^{\text{sol}} | \hat{V}_{\text{gr}}^{\text{pol}} | \Psi_{\text{gr}}^{\text{sol}} \rangle + E_{\text{gr}}^{\text{pol}}$$
(13)

Finally, the fragment—fragment electrostatic and remainder energies are $E_{\rm EFP}^{\rm coul}$ and $E_{\rm EFP}^{\rm rem}$, respectively.

Effectively, the energy contributions are computed as the expectation values of the corresponding operators over the gasphase (unpolarized) and solvated (polarized) wave functions. Applying such analysis to both the ground and electronically excited states makes it possible to decompose solvatochromic shifts into the corresponding EFP energy components, where all terms are found as differences in expectation values over the excited- and ground-state wave functions.

In the present work, we intend to decompose the interaction energy between the QM and EFP regions into both energy components and the contributions of individual solvent molecules. We formulate this decomposition for the ground electronic state and then extend the formalism to the electronically excited states and solvatochromic shifts. The principal scheme of QM/EFP PEEDA is shown in Figure 1.

Let's represent the total system energy of eq 3 as

$$E_{\text{QM/EFP,gr}} = E_{\text{QM,gr}} + E_{\text{EFP-EFP}} + E_{\text{QM-EFP,gr}}$$
(14)

The interaction energy between the QM region in the ground electronic state and the EFP subsystem can be expressed as

$$\begin{split} E_{\text{QM-EFP,gr}} &= [\langle \Psi_{\text{gr}}^{\text{sol}} | \hat{H}_{\text{QM}} | \Psi_{\text{gr}}^{\text{sol}} \rangle - \langle \Psi_{\text{gr}}^{0} | \hat{H}_{\text{QM}} | \Psi_{\text{gr}}^{0} \rangle] \\ &+ \langle \Psi_{\text{gr}}^{\text{sol}} | \hat{V}^{\text{coul}} + \hat{V}_{\text{gr}}^{\text{pol}} | \Psi_{\text{gr}}^{\text{sol}} \rangle + E_{\text{QMnuc-EFP}}^{\text{coul}} + \end{split}$$

$$E_{\text{QM-EFP,gr}}^{\text{pol}} + E_{\text{QM-EFP}}^{\text{disp}} + E_{\text{QM-EFP}}^{\text{ex-rep}}$$
(15)

The total polarization energy in eq 15 is approximately separated into the fragment—fragment $E_{\rm EFP}^{\rm pol}$ and QM-fragment $E_{\rm OM-EFP}^{\rm pol}$ components, such that

$$E_{\text{QM-EFP,gr}}^{\text{pol}} = \frac{1}{2} \sum_{a}^{x,y,z} \sum_{p} \left(-\mu_a^p F_a^{\text{QMnuc},p} + \tilde{\mu}_a^p F_a^{\text{QM},p} \right)$$
(16)

Note that this separation is approximate as the fragment—fragment polarization energies of the total (QM + EFP) system and the EFP-only system are not the same due to the QM region polarizing the EFP subsystem.

Following the definitions of ref 37 (eqs 8-13), eq 15 can be rewritten as

$$\begin{split} E_{\mathrm{QM-EFP,gr}} &= E^{\mathrm{elec}(1)} + E^{\mathrm{pol \, solute}(0)} + E^{\mathrm{pol \, solute}(1)} \\ &\quad + E^{\mathrm{pol \, frag}(0)} + E^{\mathrm{pol \, frag}(1)} + E^{\mathrm{disp}}_{\mathrm{QM-EFP}} + \\ E_{\mathrm{QM-EFP}}^{\mathrm{ex-rep}} &= [\langle \Psi_{\mathrm{gr}}^{0} | \hat{V}^{\mathrm{coul}} | \Psi_{\mathrm{gr}}^{0} \rangle + E_{\mathrm{QMnuc-EFP}}^{\mathrm{coul}}] \\ &\quad + [\langle \Psi_{\mathrm{gr}}^{\mathrm{sol}} | \hat{H}_{\mathrm{QM}} | \Psi_{\mathrm{gr}}^{\mathrm{sol}} \rangle - \langle \Psi_{\mathrm{gr}}^{0} | \hat{H}_{\mathrm{QM}} | \Psi_{\mathrm{gr}}^{0} \rangle] + \\ [\langle \Psi_{\mathrm{gr}}^{\mathrm{sol}} | \hat{V}^{\mathrm{coul}} | \Psi_{\mathrm{gr}}^{\mathrm{sol}} \rangle - \langle \Psi_{\mathrm{gr}}^{0} | \hat{V}^{\mathrm{coul}} | \Psi_{\mathrm{gr}}^{0} \rangle] \\ &\quad + [E_{\mathrm{QM-EFP,gr}}^{\mathrm{pol}} + \langle \Psi_{\mathrm{gr}}^{\mathrm{sol}} | \hat{V}_{\mathrm{gr}}^{\mathrm{pol}} | \Psi_{\mathrm{gr}}^{\mathrm{sol}} \rangle] \\ &\quad + E_{\mathrm{QM-EFP}}^{\mathrm{disp}} + E_{\mathrm{QM-EFP}}^{\mathrm{ex-rep}} \end{split}$$

with the analogous meaning of the terms (from the left to right) as the first-order electrostatic energy, the solute polarization energy of the zero and first orders, the solvent polarization energy, and the additive dispersion and exchange-repulsion terms. Now we aim to decompose the terms of eq 17 into contributions due to individual fragments. Each of the integrals involving $\hat{V}^{\rm coul}$ and $\hat{V}^{\rm pol}$ operators can be decomposed into individual fragment contributions as

$$E^{\text{elec}(1)} = \langle \Psi_{\text{gr}}^{0} | \hat{V}^{\text{coul}} | \Psi_{\text{gr}}^{0} \rangle + E_{\text{QMnuc-EFP}}^{\text{coul}}$$

$$= \sum_{A}^{\text{fragments}} [\langle \Psi_{\text{gr}}^{0} | \sum_{k \in A} \hat{V}_{k}^{\text{coul}} | \Psi_{\text{gr}}^{0} \rangle$$

$$+ \sum_{i}^{\text{QMnuc}} \sum_{k \in A} Z_{i} P_{i}^{\text{coul},k}]$$
(18)

where Z_i are nuclear charges of the QM region and $P_i^{\text{coul},k}$ are electrostatic potentials at the positions of nuclei Z_i due to EFP multipoles located at point k belonging to fragment A. A similar decomposition into the individual fragment contributions can be performed for other terms involving integrals over \hat{V}^{coul} and \hat{V}^{pol} .

Polarization energy can be approximately decomposed into individual fragment contributions as

$$E_{\text{QM-EFP,gr}}^{\text{pol}} = \sum_{A}^{\text{fragments}} \frac{1}{2} \sum_{a}^{x,y,z} \sum_{p \in A} \left(-\mu_a^p F_a^{\text{QMnuc},p} + \tilde{\mu}_a^p F_a^{\text{QM},p} \right)$$
(19)

Dispersion and exchange-repulsion terms are also pairwise-additive.

The only term that cannot be similarly split into fragment contributions is the zero-order solute polarization energy $E^{\text{pol solute}(0)} = [\langle \Psi_{\text{gr}}^{\text{sol}} | \hat{H}_{\text{QM}} | \Psi_{\text{gr}}^{\text{sol}} \rangle - \langle \Psi_{\text{gr}}^{0} | \hat{H}_{\text{QM}} | \Psi_{\text{gr}}^{0} \rangle]. \quad \text{For the}$

ground state, it is possible to decompose wave function perturbations due to individual fragments A $(\Psi_{\rm gr}^{\rm sol}=\Psi_{\rm gr}^0+\sum_{\rm A}^{\rm fragments}\delta\Psi^{\rm sol,A})$ using Roothaan step extrapolation or Newton–Raphson correction with an electronic Hessian. ^1 Perturbation theory expression can be utilized for decomposing this term for the electronically excited states (see Supporting Information), but this development is left for future work. On the other hand, the zero-order solute polarization term is expected to be the smallest. From the perturbation theory analysis (see Supporting Information), this term is about twice smaller and of the opposite sign than the second solute p o l a r i z a t i o n

 $E^{\mathrm{pol\ solute}(1)} = [\langle \Psi^{\mathrm{sol}}_{\mathrm{gr}} | \hat{V}^{\mathrm{coul}} | \Psi^{\mathrm{sol}}_{\mathrm{gr}} \rangle - \langle \Psi^{0}_{\mathrm{gr}} | \hat{V}^{\mathrm{coul}} | \Psi^{0}_{\mathrm{gr}} \rangle].$ Thus, one strategy is to exclude $E^{\mathrm{pol\ solute}(0)}$ from the decomposition and keep it as a remainder, while the other approach is to split this term between the fragments in the same proportion as $E^{\mathrm{pol\ solute}(1)}$. We will use the former strategy in the following discussion.

Now we show how to apply QM-EFP pairwise energy decomposition to the analysis of solvatochromic shifts. The QM/EFP energy of the electronically excited state in a zero-order polarizable embedding is

$$\begin{split} E_{\text{QM/EFP}}^{\text{ex,0}} &= \langle \Psi_{\text{ex}}^{\text{sol}} | \hat{H}_{\text{QM}} + \hat{V}^{\text{coul}} + \hat{V}_{\text{gr}}^{\text{pol}} | \Psi_{\text{ex}}^{\text{sol}} \rangle + E_{\text{QMnuc-EFP}}^{\text{coul}} \\ &+ E_{\text{gr}}^{\text{pol}} + E_{\text{QM-EFP}}^{\text{disp}} + E_{\text{QM-EFP}}^{\text{ex-rep}} + E_{\text{EP}}^{\text{coul}} + \end{split}$$

$$E_{\rm EFP}^{\rm disp} + E_{\rm EFP}^{\rm ex-rep} \tag{20}$$

where $\Psi_{\rm ex}^{\rm sol}$ is the wave function of the solvated excited state. In the zero-order treatment, the environment is not repolarized for the electronically excited state (hence, subscripts "gr" in $\hat{V}_{\rm gr}^{\rm pol}$ and $E_{\rm gr}^{\rm pol}$). In such an approach, the self-consistency of polarization between the QM and EFP regions is lost. However, this simple treatment has been shown to account for the majority of solvatochromic effects in polar or polarizable solvents. The explicit interaction of the excited-state electron density with the polarizable environment can be included using either linear response or state-specific approaches or their perturbative approximations. However, we will limit our discussion to the simplest zero-order model in this work. In this case, the excitation energy in the polarizable environment is

$$\Delta E_{\rm ex,0}^{\rm sol} = \langle \Psi_{\rm ex}^{\rm sol} | \hat{H}_{\rm QM} + \hat{V}^{\rm coul} + \hat{V}_{\rm gr}^{\rm pol} | \Psi_{\rm ex}^{\rm sol} \rangle - \langle \Psi_{\rm gr}^{\rm sol} | \hat{H}_{\rm QM} + \hat{V}^{\rm coul} + \hat{V}_{\rm gr}^{\rm pol} | \Psi_{\rm gr}^{\rm sol} \rangle$$
(21)

Solvatochromic (electrochromic) shift, which is a change in the excitation energy upon solvation, is defined as

$$E_{\text{soly}} = \Delta E_{\text{ex}}^{\text{sol}} - \Delta E_{\text{ex}}^{0} \tag{22}$$

where $\Delta E_{\rm ex}^{\,0}$ is the gas-phase excitation energy $\Delta E_{\rm ex}^{\,0} = \langle \Psi_{\rm ex}^0 | \hat{H}_{\rm QM} | \Psi_{\rm ex}^0 \rangle - \langle \Psi_{\rm gr}^0 | \hat{H}_{\rm QM} | \Psi_{\rm gr}^0 \rangle$ and $\Psi_{\rm gr/ex}^0$ is the gas-phase wave function of the ground/excited electronic state. In the zero-order polarizable embedding QM/EFP, a solvatochromic shift can be written as

$$\begin{split} E_{\rm solv}^{\rm QM/EFP} &= [\langle \Psi_{\rm ex}^{\rm sol} | \hat{H}_{\rm QM} + \hat{V}^{\rm coul} + \hat{V}_{\rm gr}^{\rm pol} | \Psi_{\rm ex}^{\rm sol} \rangle \\ &- \langle \Psi_{\rm ex}^{0} | \hat{H}_{\rm QM} | \Psi_{\rm ex}^{0} \rangle] - \end{split}$$

$$[\langle \Psi_{\rm gr}^{\rm sol}|\hat{H}_{\rm QM} + \hat{V}^{\rm coul} + \hat{V}_{\rm gr}^{\rm pol}|\Psi_{\rm gr}^{\rm sol}\rangle - \langle \Psi_{\rm gr}^{0}|\hat{H}_{\rm QM}|\Psi_{\rm gr}^{0}\rangle] \quad \ \ (23)$$

In the above equation, the expressions in the square brackets reflect the changes of the excited-state energy (first bracket) and ground-state energy (second bracket) upon solvation. Following the energy decomposition strategy of ref 37, the solvatochromic shift can be first decomposed as

$$\begin{split} E_{\text{solv}}^{\text{QM/EFP}} &= [E_{\text{ex}}^{\text{elec(1)}} - E_{\text{gr}}^{\text{elec(1)}}] + [E_{\text{ex}}^{\text{pol solute(0)}} \\ &- E_{\text{gr}}^{\text{pol solute(0)}}] + [E_{\text{ex}}^{\text{pol solute(1)}} - E_{\text{gr}}^{\text{pol solute(1)}}] + \\ [E_{\text{ex}}^{\text{pol frag(1)}} - E_{\text{gr}}^{\text{pol frag(1)}}] \end{split}$$

Effectively, each of the terms in the brackets provides a specific energy contribution to the solvatochromic shift. Note that the zero-order fragment polarization term in the zero-order polarizable embedding cancels out. Further, each of the terms in the square brackets (with the exception of the zero-order solute polarization term) is separated into the contributions of individual fragments. As a result, the total solvatochromic shift can be represented as

$$E_{\text{solv}}^{\text{QM/EFP}} = \sum_{A}^{\text{fragments}} (\Delta E_{\text{ex/gr}}^{\text{elec(1),A}} + \Delta E_{\text{ex/gr}}^{\text{pol solute(1),A}} + \Delta E_{\text{ex/gr}}^{\text{pol frag(1),A}}) + \Delta E_{\text{ex/gr}}^{\text{pol solute(0)}}$$
(25)

The definitions of the terms in eq 25 are

$$\Delta E_{\text{ex/gr}}^{\text{elec(1),A}} = \sum_{k \in A} \left(\langle \Psi_{\text{ex}}^{0} | \hat{V}_{k}^{\text{coul}} | \Psi_{\text{ex}}^{0} \rangle - \langle \Psi_{\text{gr}}^{0} | \hat{V}_{k}^{\text{coul}} | \Psi_{\text{gr}}^{0} \rangle \right)$$
(26)

$$\begin{split} \Delta E_{\rm ex/gr}^{\rm pol \; solute(1),A} &= \sum_{k \in \mathcal{A}} \left(\langle \Psi_{\rm ex}^{\rm sol} | \hat{V}_{k}^{\rm coul} | \Psi_{\rm ex}^{\rm sol} \rangle - \langle \Psi_{\rm ex}^{0} | \hat{V}_{k}^{\rm coul} | \Psi_{\rm ex}^{0} \rangle \right. \\ &- \langle \Psi_{\rm gr}^{\rm sol} | \hat{V}_{k}^{\rm coul} | \Psi_{\rm gr}^{\rm sol} \rangle + \langle \Psi_{\rm gr}^{0} | \hat{V}_{k}^{\rm coul} | \Psi_{\rm gr}^{0} \rangle) \end{split} \tag{27}$$

$$\Delta E_{\rm ex/gr}^{\rm pol\,frag(1),A} = \sum_{p \in \mathcal{A}} \left(\langle \Psi_{\rm ex}^{\rm sol} | \hat{V}_{p,\rm gr}^{\rm pol} | \Psi_{\rm ex}^{\rm sol} \rangle - \langle \Psi_{\rm gr}^{\rm sol} | \hat{V}_{p,\rm gr}^{\rm pol} | \Psi_{\rm gr}^{\rm sol} \rangle \right)$$
(28)

$$\begin{split} \Delta E_{\rm ex/gr}^{\rm pol \; solute(0)} &= \langle \Psi_{\rm ex}^{\rm sol} | \hat{H}_{\rm QM} | \Psi_{\rm ex}^{\rm sol} \rangle - \langle \Psi_{\rm ex}^{\rm 0} | \hat{H}_{\rm QM} | \Psi_{\rm ex}^{\rm 0} \rangle \\ &- \langle \Psi_{\rm gr}^{\rm sol} | \hat{H}_{\rm QM} | \Psi_{\rm gr}^{\rm sol} \rangle + \langle \Psi_{\rm gr}^{\rm 0} | \hat{H}_{\rm QM} | \Psi_{\rm gr}^{\rm 0} \rangle \end{split} \tag{29}$$

In the following, we will refer to these terms as the three separable terms: electrostatic (eq 26), solute polarization (eq 27), solvent polarization (eq 28), and a nonseparable portion of the solute polarization (eq 29) referred to in the following as the "dH" term.

Note that the terms in eqs 26, 27, and 29 are also present in electrostatic embedding QM/MM models (even though the exact form of the electrostatic potential $\hat{V}_k^{\rm coul}$ might be different). The fragment polarization term is specific to the polarizable embedding models. In the state-specific or linear response treatment of the polarizable embedding, fragment polarization should be additionally augmented by a term that accounts for a difference between the ground- and excited-state polarization of the solvent.

COMPUTATIONAL DETAILS

Two model systems are considered. In a local minimum of a water pentamer, shown in Figure 2, a central water molecule is

Figure 2. (a) Structure of the water pentamer: the central water, denoted as "QM", is modeled quantum-mechanically; waters W1–W4 are described with effective potentials. (b,c) Molecular orbitals of the QM water involved in the first singlet electronic excitation: (b) HOMO and (c) LUMO.

treated quantum-mechanically, while the other waters are described with effective fragments with potentials from ref 51. Polarization short-range damping functions with default Gaussian-like parameters are employed. 52 The lowest singlet excitation on the central water is modeled with the CIS/6-31G(d) level of theory.

The two lowest excitations of uracil solvated in water are discussed next. The system was initially prepared by using classical and QM/EFP1 molecular dynamics (MD) simulations. For classical simulations, one uracil molecule modeled with an OPLS-AA force field prepared using the LibParGen server^{53–55} was solvated by 5373 TIP3P water molecules in a periodic box with dimensions of ~55 Å. A series of NVE, NVT, and NPT simulations of 100 ps each were conducted to equilibrate the system in the GROMACS molecular simulation software.⁵⁶ A single snapshot of the NPT trajectory was used as a starting point for QM/EFP1 MD simulations, which were performed without periodic boundary conditions for a cluster of uracil solvated by a shell of 15 Å of water, determined by the minimal distance between any two atoms between uracil and water molecules. QM/EFP1 MD utilized NVT with the Nose-Hoover velocity rescaling algorithm and was run for 2 ps with a 0.5 fs time step. B3LYP/DZP was used for describing uracil; DFT-type EFP1 water potential ("H2ODFT")⁴⁰ was utilized to model water molecules. These simulations were performed in the GAMESS quantum chemistry package. 57,58

For the analysis of the different components of interaction energies and solvatochromic shifts, TD-DFT/EFP simulations with wB97x-d/6-31+G(d) 59,60 were performed on a single snapshot from QM/EFP1 MD and on a selection of the snapshots taken every 100 fs. EFP potentials were prepared in the 6-31G(d) basis at the geometry of the TIP3P water molecule. The convergence of solvatochromic shifts was explored by solvating uracil with water shells of different sizes, determined by the minimal distance between any two atoms between uracil and water molecules.

QM/EFP PEEDA calculations were performed in the Q-Chem quantum chemistry software ⁶¹ that incorporates EFP codes from the LibEFP software library. ^{62,63}

■ RESULTS AND DISCUSSION

Water Pentamers. Figure 2 shows the water pentamer where the central water, treated quantum-mechanically, donates two H-bonds and accepts two H-bonds to/from the four EFP waters. The considered electronic excitation is the lowest singlet state in which an electron is transferred from the water's lone pair orbital to the σ^* unoccupied orbital. In the ground electronic state, the lone pair orbital donates the electron density to H-bond donors (W2 and W3), while the unoccupied σ^* orbital accepts the electron density from waters W1 and W4. Thus, all surrounding H-bonds disfavor a shift of the electron

density from the lone pair to σ^* upon electronic excitation, such that this excitation is expected to be blue-shifted (destabilized) in this water cluster, compared to that of the gas phase. The developed pairwise analysis provides a means to decompose the total solvatochromic shift into contributions of individual water molecules, as shown in Table 1 and Figures 3 and 4. It should be

Table 1. Decomposition of Solute-Solvent Interaction Energies and Solvatochromic Shifts in the Water Pentamer^a

		W1	W2	W3	W4	total
			und State,		.,,	Cotui
elec		-7.47	-6.34	-5.41	-8.62	-27.83
solute pol	full	-7.47 -1.05	-0.34 -2.17	-3.41 -1.22	-8.02 -2.23	-27.83 -6.67
solute poi	dimers	-0.95	-2.17 -1.11	-0.83	-2.23 -1.59	-0.07 -4.48
solvent pol	full	-0.93 -1.02	-0.94	-0.66	-1.37 -1.27	-3.88
solvent poi	dimers	-0.86	-0.64	-0.44	-1.27 -1.00	-3.88 -2.94
total sep	full	-9.53	-9.44	-7.29	-1.00	-38.39
сосы эср	dimers	-9.33 -9.28	-8.09	-6.68	-12.12 -11.22	-35.27
dH	full	7.20	0.07	0.00	11.22	3.92
	dimers	0.56	0.63	0.46	0.92	2.57
total	full	3.30	0.00	5.10	3.72	-34.46
	dimers	-8.71	-7.45	-6.22	-10.29	-32.67
Excited State, S ₁						
elec		3.77	2.03	5.18	3.82	14.8
solute pol	full	2.31	-2.96	-1.25	-7.44	-9.34
	dimers	-9.25	-1.43	-1.03	-15.03	-26.74
solvent pol	full	2.39	1.01	1.11	0.17	4.68
	dimers	-0.63	0.85	0.87	-1.25	-0.16
total sep	full	8.48	0.08	5.04	-3.45	10.15
	dimers	-6.10	1.45	5.02	-12.46	-12.09
dH	full					-2.96
	dimers	2.86	-1.29	-0.89	5.27	5.95
total	full					7.18
	dimers	-3.24	0.16	4.13	-7.19	-6.14
Solvatochromic Shifts, S_1 – S_0						
elec		11.24	8.36	10.58	12.44	42.63
solute pol	full	3.36	-0.80	-0.02	-5.21	-2.67
	dimers	-8.31	-0.32	-0.20	-13.44	-22.27
solvent pol	full	3.4	1.95	1.77	1.44	8.57
	dimers	0.24	1.49	1.31	-0.25	2.79
total sep	full	18.01	9.52	12.33	8.67	48.53
	dimers	3.17	9.53	11.7	-1.24	23.16
dH	full					-6.88
	dimers	2.30	-1.92	-1.35	4.35	3.38
total	full					41.65
	dimers	5.47	7.62	10.34	3.11	26.54

^aThe energies of separable electrostatic (elec), solute polarization (solute pol), solvent polarization (solvent pol) terms, their sum (total sep), and non-separable solute polarization (dH) components are given in kcal/mol.

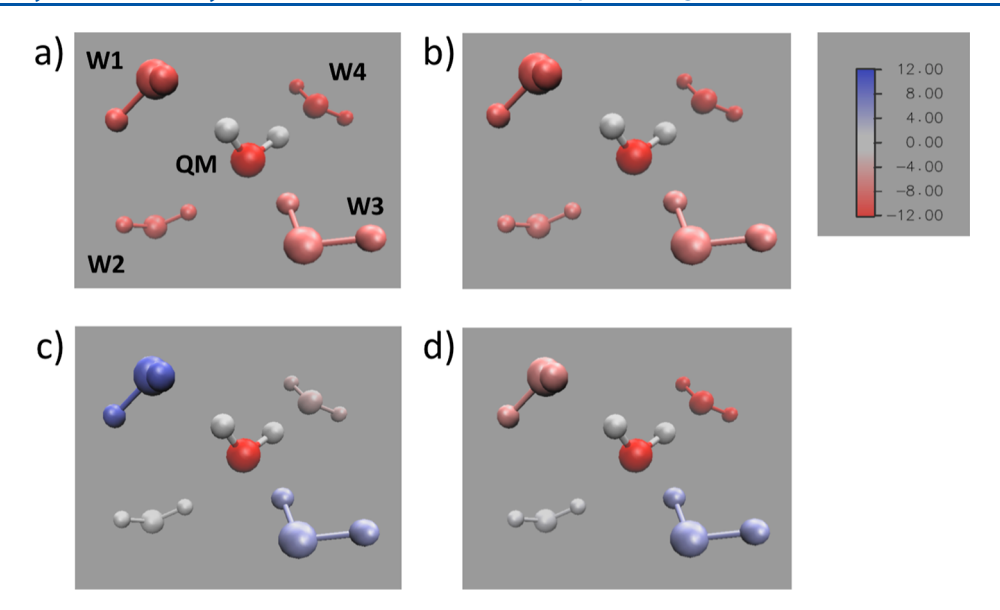


Figure 3. Total separable components of the interaction energies of the central (QM) water molecule with each of the four other waters in the ground electronic state, shown in (a,b), and in the first excited state, shown in (c,d). The system is computed as one entity ("full system", i.e., the QM water and four EFP waters) in plots (a,c). Four dimers (each containing the QM water and one EFP water) are computed separately in (b,d). The interaction energy color scale is ± 12 kcal/mol.

noted that the total absorption spectrum of this water cluster is composed of five excitonic bands that can be computed by considering the excitonic Hamiltonian containing excitation (site) energies of each water molecule and electronic couplings between them, as was extensively discussed in the literature. ^{10,14,15,33} On the other hand, PEEDA can provide a decomposition of the solvatochromic shifts on each of the water molecules (i.e., decomposition of solvent-induced changes to the site energies in the excitonic Hamiltonian), as we demonstrate below for the central water molecule.

The upper parts of Table 1 and Figures 3a,b and 4a present the electrostatic and polarization components of the interaction energies of the central water molecule with each of the four other waters in the ground electronic state. Two sets of calculations are compared: in the first one, the system is computed as one entity ("full system", i.e., the QM water and four EFP waters); in the other, four dimers (each containing the QM water and one EFP water) are computed separately. Effectively, the difference between these sets of calculations is a QM-EFP many-body interaction energy. The pairwise electrostatic energies are identical in two sets of calculations. Polarization amounts to about a third of the electrostatic energy and is split in a similar proportion between the solute and solvent polarization (note that the nonseparable dH component is a part of the solute polarization energy). As expected, the nonseparable solute polarization energy dH is about twice smaller in magnitude and of the opposite sign than the separable solute polarization term (see Supporting Information). Overall, the results of the calculations on the entire system and the dimers are very similar, with the individual contributions differing by less than 1.4 kcal/mol and the total (electrostatic and polarization) interaction energies between the central water and all others within 2 kcal/mol of each other. These results agree with common sense that waters W1-W4 do not strongly polarize each other such that the many-body interactions in this system play a minor role. Additionally, this analysis is in accord with previous findings from the SAPT analysis that separating the system into dimers provides almost quantitative agreement in

predicting ligand-binding energies.⁶⁴ However, as we will see next, the situation is dramatically different for the electronic excited state.

The middle parts of Table 1 and Figures 3c,d and 4b show the full-system and dimer calculations of the interaction energies between the central water in the first electronically excited state and the four other EFP waters. The lowest parts of Table 1 and Figure 4c report the corresponding differences between the ground and excited electronic states, which are direct measures of the solvatochromic shifts. As expected from the analysis of the involved molecular orbitals, both the electrostatic term and the solvent part of polarization become strongly destabilized in the excited state. On the other hand, the (always negative) solute part of the polarization, i.e., relaxation of the wave function in response to solvent perturbation, increases in magnitude and partially compensates for this destabilization. However, differently from the ground state, there is a significant difference between describing the system as one entity or as a collection of the dimers. Indeed, modeling the system as a collection of the dimers results in the dramatically overestimated solute polarization energy (i.e., a relaxation of the wave function in response to the four EFP waters is smaller than a sum of relaxations due to each water in the dimer calculations), as well as less repulsive solvent polarization. As a result, overstabilization of the polarization terms leads to a 13 kcal/mol underestimation of the blue shift in the dimer calculations. Even more disturbing is a lack of consistency in the individual solvatochromic shifts between the entire system and dimer calculations. For example, the dimer calculations suggest that the most significant contribution to the solvatochromic shift is from W3, followed by W2, while the full system calculations show that W1 provides by far the largest contribution. There is also no correlation between the pairwise electrostatic terms and the corresponding solvatochromic shifts (even though the total electrostatic term is very similar to the total solvatochromic shift, most probably by coincidence). For example, the largest pairwise electrostatic contribution to the solvatochromic shift comes from W4, which is predicted to produce the smallest overall solvatochromic shift.

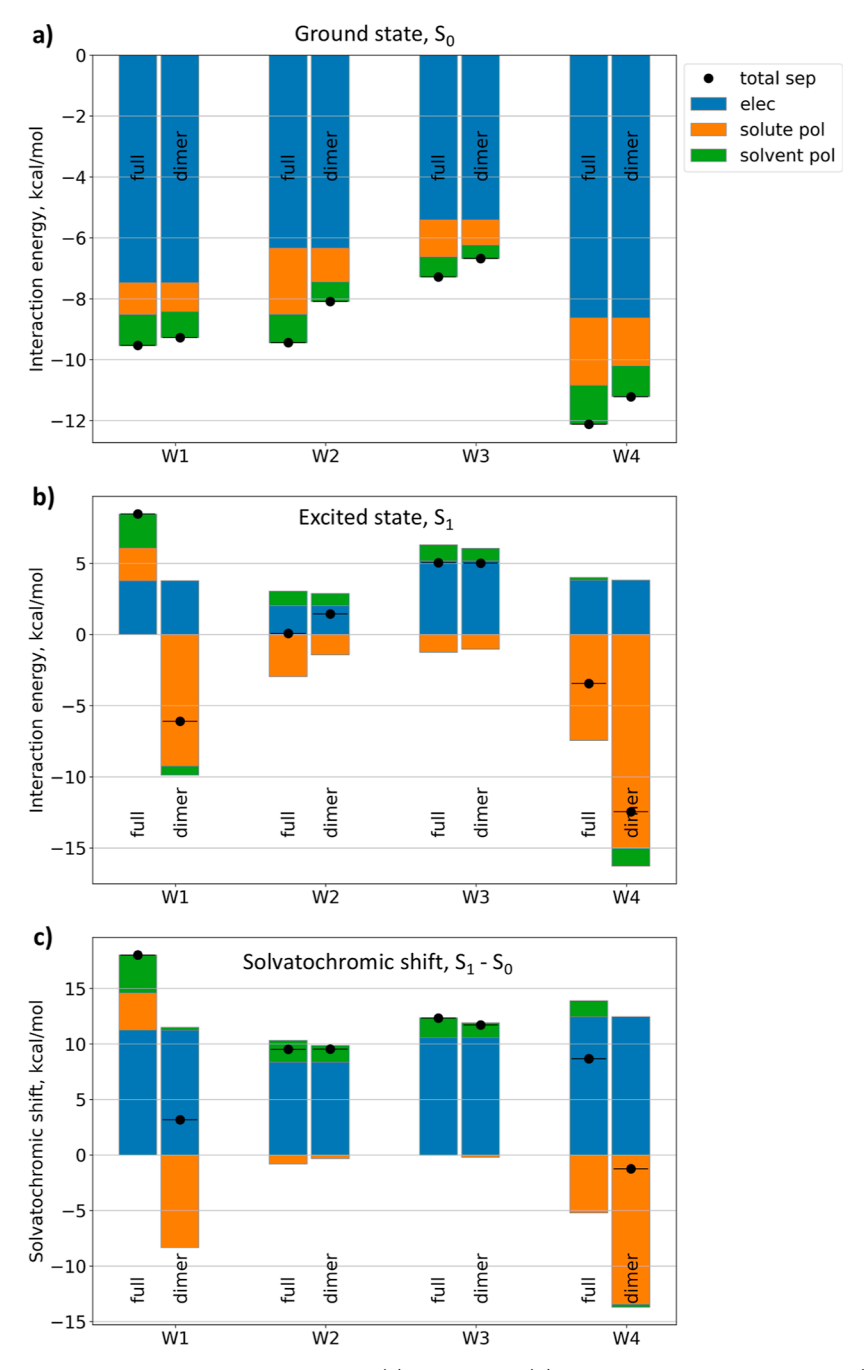


Figure 4. Decomposition of solute—solvent interaction energies in (a) ground and (b) electronically excited states and (c) solvatochromic shifts in water pentamer. Energies of separable electrostatic (elec), solute polarization (solute pol), solvent polarization (solvent pol) terms, and their sum (total sep) are shown for a full QM/EFP system and individual QM/EFP dimers.

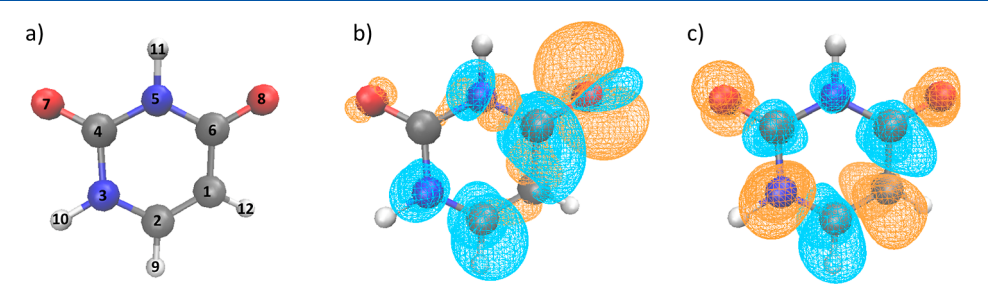


Figure 5. (a) Uracil molecule and density difference plots for (b) $n \to \pi^*$ and (c) $\pi \to \pi^*$ electronic transitions, shown at 0.002 isosurface values. Detachment density is shown in orange; attachment density is shown in cyan.

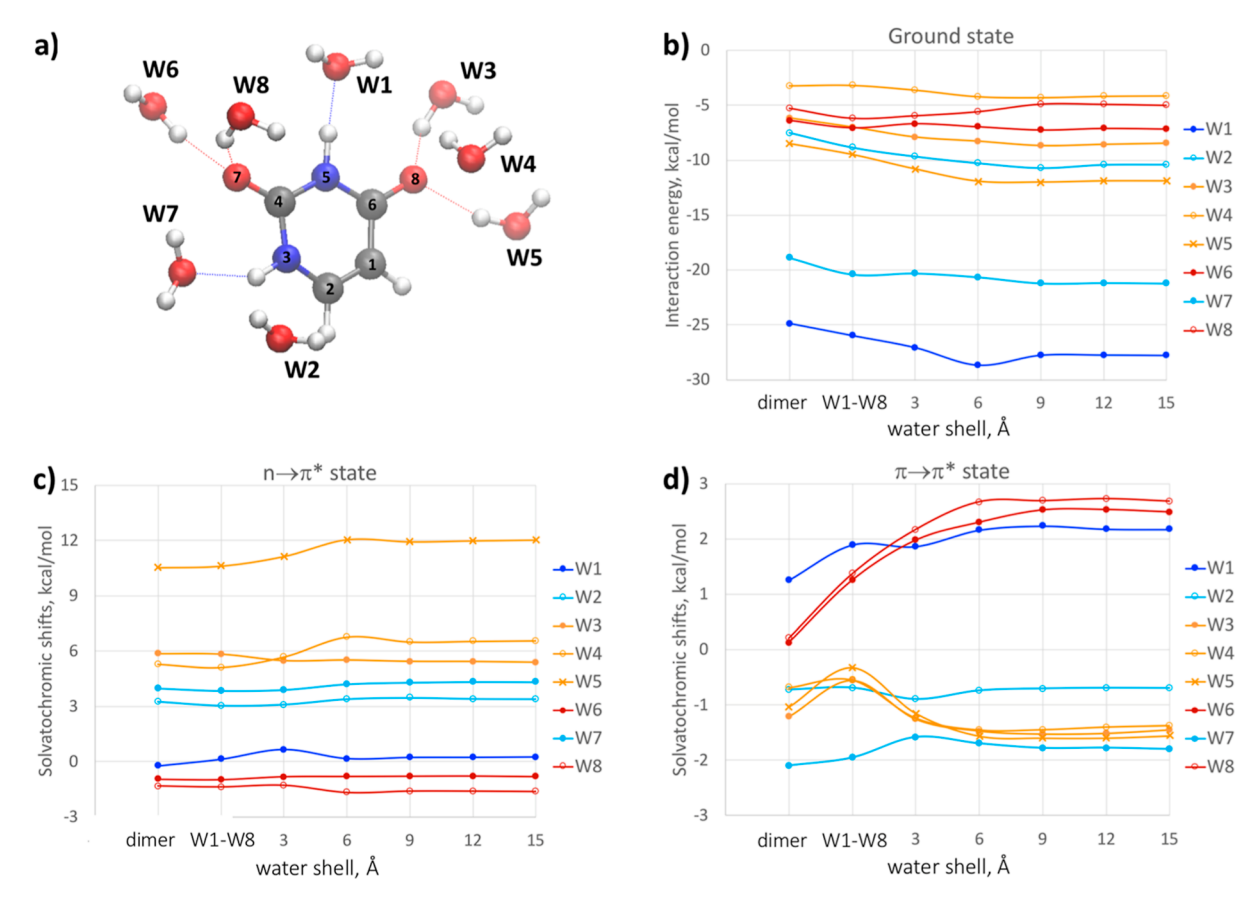


Figure 6. (a) First shell of water molecules strongly interacting with uracil and their individual (b) ground-state interaction energies and solvatochromic shifts in (b) $n \to \pi^*$ and (c) $\pi \to \pi^*$ excited states of uracil computed in the presence of a given water molecule only ("dimer"), in the presence of eight first-shell water molecules ("W1–W8"), and in the presence of other water molecules within a particular distance from uracil (3–15). All values are in kcal/mol.

These comparisons hint at a much larger amount of the many-body interactions in the electronically excited state, which makes the dimer analysis of the solvatochromic shifts unreliable. It should be emphasized that these many-body interactions are mainly driven by the response of the QM wave function rather than that of the polarizable solvent, such that these conclusions would remain unchanged even in the case of a nonpolarizable solvent in an electrostatic QM/MM model.

As a side note, the data in Table 1 suggest that in the electronically excited state, the nonseparable term dH cannot be easily related to the solute polarization term, neither by magnitude nor sign (see Supporting Information for the corresponding discussion). However, its magnitude is still relatively minor, and the most logical solution is to exclude the dH term from the analysis of the individual solvatochromic shifts

Hydrated Uracils. The two lowest singlet excited states of uracil solvated in water are analyzed below. The electronic structure of uracil in a water environment was studied previously. $^{37,65-70}$ The lowest excitation in the gas phase is a dark $n \to \pi^*$ transition; the second excited state is a bright $\pi \to \pi^*$ transition (see Figure 5). In the case of the zero-order approximation and state-specific corrections, the solvatochromic shift is induced solely by a change in the static charge rearrangement of a solute. (In the linear-response approach, the additional solvatochromic shift due to a polarizable environment is caused by a transition density.) Analysis of the static charge distributions of the gas-phase uracil (visualized as density

difference plots in Figure 5b,c) suggests that upon n $\rightarrow \pi^*$ excitation, the electron density is shifted from carbonyl oxygen O8 toward carbons C6 and C2 and to a lesser extent to nitrogens N3 and N5. There is a smaller charge rearrangement in the bright $\pi \to \pi^*$ state, with electron density depleting nitrogen N3, carbon C1, and oxygens O7 and O8 toward carbons C2 and C6. Both oxygens in uracil donate electron density when forming Hbonds with water, while the nitrogens accept electron density when forming H-bonds with water solvent. Thus, the n $\rightarrow \pi^*$ excitation is expected to be destabilized in the water solvent (since the excitation removes the electron density from oxygen O8 and adds the density toward both nitrogens), with the water molecule H-bonded to O8 being a major source of a blue shift. A weak destabilization of the $\pi \to \pi^*$ state is expected due to water H-bonded to O7, but waters H-bonded to N3 and O8 would contribute to a weak redshift. The average values of the $n \to \pi^*$ and $\pi \to \pi^*$ solvatochromic shifts predicted by QM/EFP are 0.43 and -0.25 eV, respectively, in agreement with this analysis and theoretical and experimental work.^{37,65–74} Details of these calculations are listed in Supporting Information.

Figure 6 shows the contributions of selected first-shell water molecules to the interaction energies and solvatochromic shifts of uracil solvated by a shell of water molecules of increasing size. These results are obtained at the geometries extracted from a single QM/EFP1 MD snapshot. To model water shells of different radii, water molecules beyond particular distances (e.g., 3 and 6 Å) from uracil atoms are stripped off. In the ground state, water H-bonding with N centers of uracil, shown with blue and

light-blue colors in Figure 6b, is significantly stronger than that with oxygen. The largest contribution to the blue shift of the $n \rightarrow$ π^* state arises from waters H-bonded to O8 (shown with orange colors in Figure 6c), as anticipated from the analysis of the density difference plots in Figure 5b. The water molecules near C2 and N3 also destabilize the n $\rightarrow \pi^*$ state, while the water molecules near O7 and N5 provide no or weak stabilization. For the $\pi \to \pi^*$ state (Figure 6d), the water molecules H-bonded to N3 and N5 shift the excited state toward lower and higher energies, respectively, in agreement with expectations from the density difference plots. However, the waters H-bonded to O7 and O8, while expected to destabilize the $\pi \to \pi^*$ state, in reality provide small shifts of different signs. This might be rationalized by a partial interaction of those waters with the electron densities of nearby carbons C4 and C6 and non-negligible and nonlinear solute polarization contributions.

Figure 6 also shows the dependence of individual fragment interaction energies and solvatochromic shifts on the presence of surrounding water molecules. As follows from these plots, the individual water contributions converge in the presence of ~9 Å of water shell, suggesting non-negligible and long-range polarization effects. Changes in the individual contributions from the dimer to the fully solvated value can be as much as 3 kcal/mol for the ground state and exceeding 1.5 kcal/mol and 2.5 kcal/mol for the n $\rightarrow \pi^*$ and $\pi \rightarrow \pi^*$ states, respectively. As a result, the difference between the sum of the dimer interaction energies and the contributions of these eight waters in a fully solvated system is ~15 kcal/mol for the ground state, ~3 kcal/ mol for the n $\rightarrow \pi^*$ state, and almost \sim 5 kcal/mol for the $\pi \rightarrow \pi^*$ state. Overall, Figure 6d demonstrates a striking interplay of polarization effects in the $\pi \to \pi^*$ state, which might explain the challenges of its accurate description discussed in the literature.65

Figure 7 presents the decomposition of interaction energies and solvatochromic shifts of uracil into physical energy components, computed at the same structures as those of the data shown in Figure 6. As expected, in the ground electronic state of uracil (Figure 7a), the uracil-water interactions are dominated by electrostatics (~-60 kcal/mol); however, both solute and solvent polarization terms contribute significantly. The nonseparable dH component is the only repulsive term; the magnitude of dH is ~1.5 times smaller than the magnitude of the solute polarization energy. A sum of separable contributions (electrostatics, solute, and solvent polarizations) overestimates the total interaction energy by \sim 20%. It qualitatively reproduces the changes in the total energy with the increase in the solvation shell size. Overall, all interaction components show monotonic behavior with the increase of the solvation shell radius; the results at the 6 Å hydration shell are within 1 kcal/mol from the results at the 12 and 15 Å water shells.

Figure 7b,c shows the decomposition of solvatochromic shifts for $n \to \pi^*$ and $\pi \to \pi^*$ electronic excited states, respectively. Since these are vertical shifts, i.e., the effect of geometry relaxation of uracil in water solvent is not accounted for, all observed trends should be considered qualitative. As was discussed earlier, the $n \to \pi^*$ state is strongly destabilized by the water solvent, with the total solvatochromic shift exceeding 20 kcal/mol. Similar to the ground-state interaction energy, the $n \to \pi^*$ solvatochromic shift is dominated by the electrostatic term, with the solvent polarization being non-negligible. However, the solvent electrostatic and polarization effects are halved by the wave function relaxation represented by the nonseparable dH term, while the separable solute polarization

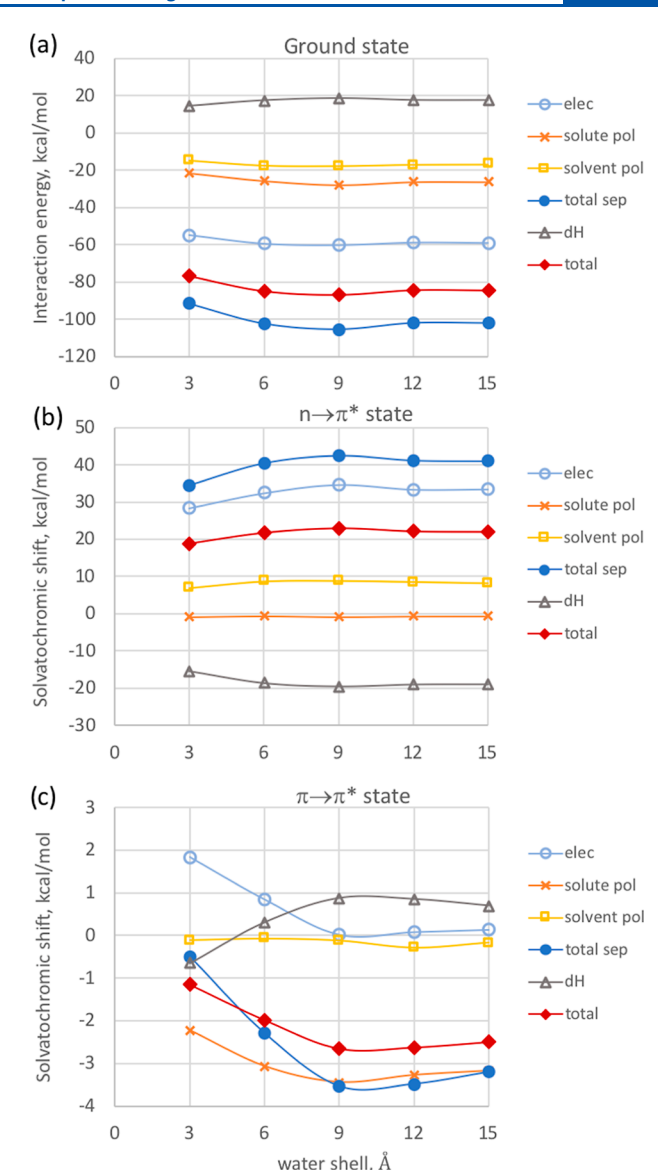


Figure 7. (a) QM–EFP ground-state interaction energy and solvatochromic shifts for (b) n $\rightarrow \pi^*$ and (c) $\pi \rightarrow \pi \rightarrow \pi^*$ excited states of uracil as a function of the surrounding water shell size. Energy decomposition in electrostatic (light blue empty circles), solute polarization (orange crosses), solvent polarization (light orange empty squares), total separable contributions (dark blue filled circles), nonseparable dH component (gray triangles), and total energies (red rhombuses). All values are in kcal/mol.

term is negligible. Differently from the ground-state interaction, in the case of solvatochromic shifts of excited states, there is no clear correlation between separable solute polarization and dH terms. However, the dH term and total separable energy scale similarly with the size of the water shell, suggesting that this relation might be qualitatively true for individual water molecules as well.

Analysis of solvatochromic shifts in $\pi \to \pi^*$ reveals a picture quite different from that of the n $\to \pi^*$ shifts. The $\pi \to \pi^*$ state is destabilized by electrostatic interactions in the first hydration shell that are counteracted by mid- and long-range interactions. The effect of water polarization is negligible. Interestingly, the sign and magnitude of the solvatochromic shift in $\pi \to \pi^*$ are determined by the attractive solute polarization term with a nonnegligible midrange component. Additionally, the distance

dependence of the solvatochromic effect is much more pronounced in $\pi \to \pi^*$ than in $n \to \pi^*$ (even though note that the vertical energy scale differs by an order of magnitude in the plots of the two states).

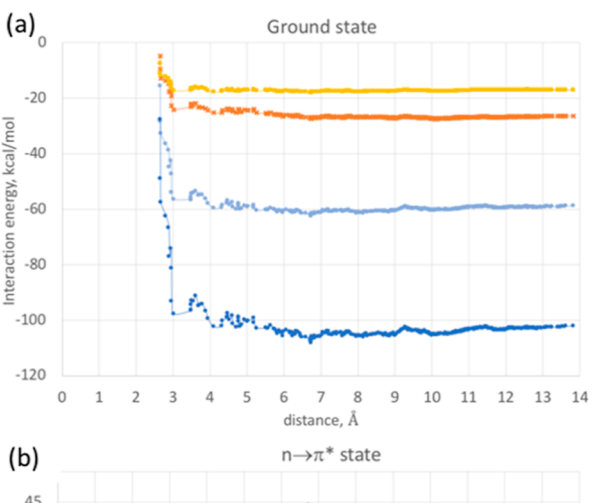
To further elucidate the distance dependence of solvatochromic shifts, Figure 8 shows decompositions of the ground-state interaction energy and the n $\rightarrow \pi^*$ and $\pi \rightarrow \pi^*$ shifts into contributions of individual water molecules. The energy decomposition is performed for a single snapshot containing a 12 Å water shell. A similar analysis of the data averaged over ten structural snapshots is shown in Figure S1 in Supporting Information. While averaging quite expectedly eliminates some fluctuations in the data, distance dependences of interaction energies and shifts still preserve characteristic "wiggles" originating due to the water structure around the uracil. To highlight the dependence of the solvatochromic shifts on water structure, the radial distribution function between nitrogen and oxygen atoms of uracil and water oxygens is provided in Figure 8d. As follows from Figure 8a, the ground-state uracil-water interaction energy is governed by water contributions in the first hydration shell, corresponding to the ~2.8 Å peak in the uracil water radial distribution function, i.e., waters participating in Hbonding with uracil. The interactions with the water molecules in the second hydration shell ($\sim 3.0 \div 5.5 \text{ Å}$) can be both stabilizing and destabilizing. The interaction energy converges to within 1 kcal/mol only beyond 12 Å. As for the contributions of individual waters, interactions of 1 kcal/mol occur even at a 7 Å uracil—water separation.

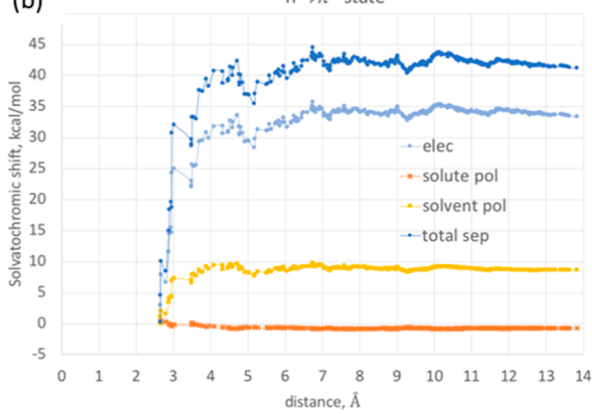
The electrostatic component of the $n \to \pi^*$ solvatochromic shift (Figure 8b) is almost a mirror image of the ground-state electrostatic energy. Namely, most of the neighboring waters strongly destabilize the $n \to \pi^*$ state (as they stabilized the ground state), with a nonmonotonic convergence of the electrostatic component and an overall solvatochromic shift beyond 12 Å. Polarization components are converged within 0.5 kcal/mol beyond 7 Å.

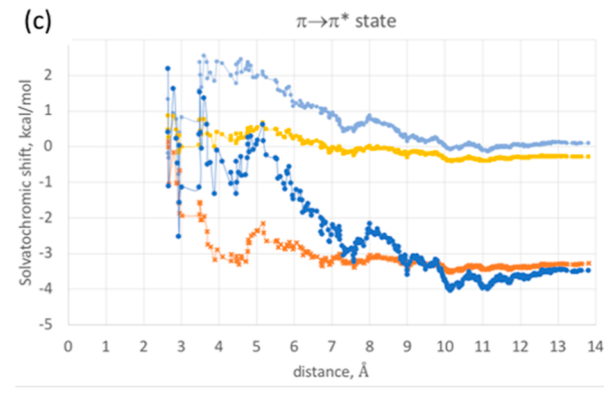
As mentioned above, the decomposition of the $\pi \to \pi^*$ solvatochromic shift, shown in Figure 8c, is very intriguing. One can notice a nonmonotonic change of various energy components with distance. Most of the short-range electrostatic contributions of individual water molecules are repulsive, while the mid- and long-range electrostatic interactions are slightly attractive. On the other hand, the largest effect of solute polarization is achieved due to the waters located in the first and partly second hydration shells. The total separable energy, which in the case of the $\pi \to \pi^*$ state is dominated by these two energy terms, strongly fluctuates with the distance. Despite a relatively small magnitude of the total solvatochromic shift, the convergence of the shift with distance is slow, with $\sim 1~\rm kcal/$ mol fluctuations observed at 10 Å from uracil.

CONCLUSIONS

We developed a new pairwise energy decomposition analysis targeting the solvatochromic shifts of solvated chromophores. The energy decomposition is implemented for the polarizable QM/EFP method and provides a decomposition of solvatochromic shifts both in the contributions of individual solvent molecules and in the electrostatic, solute polarization, and solvent polarization energy components. The new tool allows analysis of specific solute—solvent interactions in the ground and excited states, which opens new avenues for functional design of materials with target photochemical properties. We envision the application of the developed energy decomposition scheme for







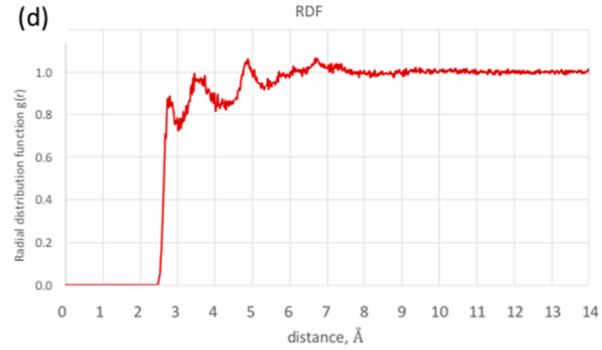


Figure 8. Contributions of individual solvent water molecules to (a) QM—EFP ground-state interaction energy and solvatochromic shifts in (b) $n \to \pi^*$ and (c) $\pi \to \pi^*$ excited states of uracil. Energy decomposition in electrostatic (light blue empty circles), solute polarization (orange crosses), solvent polarization (light orange squares), and total separable energies (dark blue filled circles). All values are in kcal/mol. (d) Radial distribution function g(R) between N and O atoms of uracil and water oxygens.

the mechanistic analysis of the optical properties of photoactive proteins and photovoltaic materials.

Analysis of solvatochromic shifts in considered model systems suggests that the solute polarization, i.e., a response of the quantum wave function to the electric field of the surrounding solvent, might be strongly nonadditive. Additionally, individual-molecule solvatochromic contributions are affected by the presence of several shells of other solvent molecules, pinpointing the importance of proper accounting and analysis of long-range polarization effects in excited-state calculations of solvated systems.

ASSOCIATED CONTENT

5 Supporting Information

The Supporting Information is available free of charge at https://pubs.acs.org/doi/10.1021/acs.jpca.3c06194.

Perturbation theory analysis of the solute polarization terms, description of the computations of the average solvatochromic shifts in uracil, and averaged contributions of the individual solvent water molecules to ground-state interaction energy and solvatochromic shifts (PDF)

AUTHOR INFORMATION

Corresponding Author

Lyudmila V. Slipchenko — Department of Chemistry, Purdue University, West Lafayette, Indiana 47906, United States; orcid.org/0000-0002-0445-2990; Email: lslipchenko@purdue.edu

Complete contact information is available at: https://pubs.acs.org/10.1021/acs.jpca.3c06194

Notes

The author declares no competing financial interest.

ACKNOWLEDGMENTS

L.V.S. acknowledges the support of the National Science Foundation (grant #CHE-2102639). This research was supported in part through the computational resources provided by the Information Technology Department at Purdue University, West Lafayette, Indiana.

REFERENCES

- (1) Horn, P. R.; Sundstrom, E. J.; Baker, T. A.; Head-Gordon, M. Unrestricted Absolutely Localized Molecular Orbitals for Energy Decomposition Analysis: Theory and Applications to Intermolecular Interactions Involving Radicals. *J. Chem. Phys.* **2013**, *138*, 134119.
- (2) Fedorov, D. G.; Kitaura, K. Pair Interaction Energy Decomposition Analysis. *J. Comput. Chem.* **2007**, 28, 222–237.
- (3) Green, M. C.; Fedorov, D. G.; Kitaura, K.; Francisco, J. S.; Slipchenko, L. V. Open-Shell Pair Interaction Energy Decomposition Analysis (PIEDA): Formulation and Application to the Hydrogen Abstraction in Tripeptides. *J. Chem. Phys.* **2013**, *138*, 074111.
- (4) Parrish, R. M.; Parker, T. M.; Sherrill, C. D. Chemical Assignment of Symmetry-Adapted Perturbation Theory Interaction Energy Components: The Functional-Group SAPT Partition. *J. Chem. Theory Comput.* **2014**, *10*, 4417–4431.
- (5) Lao, K. U.; Herbert, J. M. Accurate and Efficient Quantum Chemistry Calculations for Noncovalent Interactions in Many-Body Systems: The XSAPT Family of Methods. *J. Phys. Chem. A* **2015**, *119*, 235–252.
- (6) Hughes, J. M.; Hutter, M. C.; Reimers, J. R.; Hush, N. S. Modeling the Bacterial Photosynthetic Reaction Center. 4. The Structural,

- Electrochemical, and Hydrogen-Bonding Properties of 22 Mutants of Rhodobacter Sphaeroides. *J. Am. Chem. Soc.* **2001**, *123*, 8550–8563.
- (7) Mironov, V. A.; Khrenova, M. G.; Grigorenko, B. L.; Savitsky, A. P.; Nemukhin, A. V. Thermal Isomerization of the Chromoprotein Asfp595 and Its Kindling Mutant A143g: QM/MM Molecular Dynamics Simulations. *J. Phys. Chem. B* **2013**, *117*, 13507–13514.
- (8) Armengol, P.; Gelabert, R.; Moreno, M.; Lluch, J. M. Theoretical Computer-Aided Mutagenic Study on the Triple Green Fluorescent Protein Mutant S65t/H148d/Y145f. *ChemPhysChem* **2015**, *16*, 2134–2139.
- (9) Srivastava, A.; Ahad, S.; Wat, J. H.; Reppert, M. Accurate Prediction of Mutation-Induced Frequency Shifts in Chlorophyll Proteins with a Simple Electrostatic Model. *J. Chem. Phys.* **2021**, *155*, 151102.
- (10) Kim, Y.; Mitchell, Z.; Lawrence, J.; Morozov, D.; Savikhin, S.; Slipchenko, L. V. Predicting Mutation-Induced Changes in the Electronic Properties of Photosynthetic Proteins from First Principles: The Fenna-Matthews-Olson Complex Example. *J. Phys. Chem. Lett.* **2023**, *14*, 7038–7044.
- (11) Reppert, M. Bioexcitons by Design: How Do We Get There? *J. Phys. Chem. B* **2023**, *127*, 1872–1879.
- (12) Kimber, P.; Plasser, F. Energy Component Analysis for Electronically Excited States of Molecules: Why the Lowest Excited State Is Not Always the HOMO/LUMO Transition. *J. Chem. Theory Comput.* **2023**, *19*, 2340–2352.
- (13) Zhao, R.; Hettich, C.; Zhang, J.; Liu, M.; Gao, J. Excimer Energies. J. Phys. Chem. Lett. 2023, 14, 2917–2926.
- (14) Mata, R. A.; Stoll, H.; Cabral, B. J. C. A Simple One-Body Approach to the Calculation of the First Electronic Absorption Band of Water. *J. Chem. Theory Comput.* **2009**, *5*, 1829–1837.
- (15) Kaliakin, D. S.; Nakata, H.; Kim, Y.; Chen, Q.; Fedorov, D. G.; Slipchenko, L. V. Fmoxfmo: Elucidating Excitonic Interactions in the Fenna-Matthews-Olson Complex with the Fragment Molecular Orbital Method. *J. Chem. Theory Comput.* **2020**, *16*, 1175–1187.
- (16) Gordon, M. S.; Slipchenko, L. V.; Li, H.; Jensen, J. H. Chapter 10 The Effective Fragment Potential: A General Method for Predicting Intermolecular Interactions. *Annu. Rep. Comput. Chem.* **2007**, *3*, 177–193.
- (17) Gordon, M. S.; Smith, Q. A.; Xu, P.; Slipchenko, L. V. Accurate First Principles Model Potentials for Intermolecular Interactions. *Annu. Rev. Phys. Chem.* **2013**, *64*, 553–578.
- (18) Slipchenko, L. V.; Gurunathan, P. K. Effective Fragment Potential Method: Past, Present, and Future. In *Fragmentation: Toward Accurate Calculations on Complex Molecular Systems*; Gordon, M. S., Ed.; Wiley, 2017; pp 183–208.
- (19) Slipchenko, L. V. Solvation of the Excited States of Chromophores in Polarizable Environment: Orbital Relaxation Versus Polarization. *J. Phys. Chem. A* **2010**, *114*, 8824–8830.
- (20) DeFusco, A.; Minezawa, N.; Slipchenko, L. V.; Zahariev, F.; Gordon, M. S. Modeling Solvent Effects on Electronic Excited States. *J. Phys. Chem. Lett.* **2011**, *2*, 2184–2192.
- (21) Slipchenko, L. V. Effective Fragment Potential Method. In *Many-Body Effects and Electrostatics in Biomolecules*; Cui, Q., Meuwly, M., Ren, P., Eds.; CRC Press, 2016; pp 147–190.
- (22) Day, P. N.; Jensen, J. H.; Gordon, M. S.; Webb, S. P.; Stevens, W. J.; Krauss, M.; Garmer, D.; Basch, H.; Cohen, D. An Effective Fragment Method for Modeling Solvent Effects in Quantum Mechanical Calculations. *J. Chem. Phys.* **1996**, *105*, 1968–1986.
- (23) Gordon, M. S.; Freitag, M. A.; Bandyopadhyay, P.; Jensen, J. H.; Kairys, V.; Stevens, W. J. The Effective Fragment Potential Method: A QM-Based MM Approach to Modeling Environmental Effects in Chemistry. *J. Phys. Chem. A* **2001**, *105*, 293–307.
- (24) Ghosh, D.; Kosenkov, D.; Vanovschi, V.; Williams, C. F.; Herbert, J. M.; Gordon, M. S.; Schmidt, M. W.; Slipchenko, L. V.; Krylov, A. I. Noncovalent Interactions in Extended Systems Described by the Effective Fragment Potential Method: Theory and Application to Nucleobase Oligomers. J. Phys. Chem. A 2010, 114, 12739–12754.

- (25) Gordon, M. S.; Fedorov, D. G.; Pruitt, S. R.; Slipchenko, L. V. Fragmentation Methods: A Route to Accurate Calculations on Large Systems. *Chem. Rev.* **2012**, *112*, 632–672.
- (26) Jeziorski, B.; Moszynski, R.; Ratkiewicz, A.; Rybak, S.; Szalewicz, K.; Williams, H. L. Sapt: A Program for Many-Body Symmetry-Adapted Perturbation Theory Calculations of Intermolecular Interaction Energies. *Methods Tech. Comput. Chem.* **1993**, *94*, 79.
- (27) Parker, T. M.; Burns, L. A.; Parrish, R. M.; Ryno, A. G.; Sherrill, C. D. Levels of Symmetry Adapted Perturbation Theory (SAPT). I. Efficiency and Performance for Interaction Energies. *J. Chem. Phys.* **2014**, *140*, 094106.
- (28) Slipchenko, L. V.; Gordon, M. S.; Ruedenberg, K. Dispersion Interactions in Qm/Efp. J. Phys. Chem. A 2017, 121, 9495–9507.
- (29) Viquez Rojas, C. I.; Fine, J.; Slipchenko, L. V. Exchange-Repulsion Energy in Qm/Efp. J. Chem. Phys. 2018, 149, 094103.
- (30) Viquez Rojas, C. I.; Slipchenko, L. V. Exchange Repulsion in Quantum Mechanical/Effective Fragment Potential Excitation Energies: Beyond Polarizable Embedding. *J. Chem. Theory Comput.* **2020**, *16*, 6408–6417.
- (31) Gurunathan, P. K.; Acharya, A.; Ghosh, D.; Kosenkov, D.; Kaliman, I.; Shao, Y.; Krylov, A. I.; Slipchenko, L. V. Extension of the Effective Fragment Potential Method to Macromolecules. *J. Phys. Chem. B* **2016**, *120*, 6562–6574.
- (32) Kim, Y.; Bui, Y.; Tazhigulov, R. N.; Bravaya, K. B.; Slipchenko, L. V. Effective Fragment Potentials for Flexible Molecules: Transferability of Parameters and Amino Acid Database. *J. Chem. Theory Comput.* **2020**, *16*, 7735–7747.
- (33) Kim, Y.; Morozov, D.; Stadnytskyi, V.; Savikhin, S.; Slipchenko, L. V. Predictive First-Principles Modeling of a Photosynthetic Antenna Protein: The Fenna-Matthews-Olson Complex. *J. Phys. Chem. Lett.* **2020**, *11*, 1636–1643.
- (34) Tazhigulov, R. N.; Gurunathan, P. K.; Kim, Y.; Slipchenko, L. V.; Bravaya, K. B. Polarizable Embedding for Simulating Redox Potentials of Biomolecules. *Phys. Chem. Chem. Phys.* **2019**, *21*, 11642–11650.
- (35) Jacob, C. R.; Neugebauer, J. Subsystem Density-Functional Theory. Wiley Interdiscip. Rev. Comput. Mol. Sci. 2014, 4, 325–362.
- (36) Neugebauer, J.; Louwerse, M. J.; Baerends, E. J.; Wesolowski, T. A. The Merits of the Frozen-Density Embedding Scheme to Model Solvatochromic Shifts. *J. Chem. Phys.* **2005**, *122*, 094115.
- (37) DeFusco, A.; Ivanic, J.; Schmidt, M. W.; Gordon, M. S. Solvent-Induced Shifts in Electronic Spectra of Uracil. *J. Phys. Chem. A* **2011**, 115, 4574–4582.
- (38) Li, H.; Gordon, M. S.; Jensen, J. H. Charge Transfer Interaction in the Effective Fragment Potential Method. *J. Chem. Phys.* **2006**, *124*, 214108.
- (39) Xu, P.; Gordon, M. S. Charge Transfer Interaction Using Quasiatomic Minimal-Basis Orbitals in the Effective Fragment Potential Method. *J. Chem. Phys.* **2013**, *139*, 194104.
- (40) Adamovic, I.; Freitag, M. A.; Gordon, M. S. Density Functional Theory Based Effective Fragment Potential Method. *J. Chem. Phys.* **2003**, *118*, 6725–6732.
- (41) Sodt, A. J.; Mei, Y.; König, G.; Tao, P.; Steele, R. P.; Brooks, B. R.; Shao, Y. Multiple Environment Single System Quantum Mechanical/Molecular Mechanical (MESS-QM/MM) Calculations. 1. Estimation of Polarization Energies. *J. Phys. Chem. A* **2015**, *119*, 1511–1523.
- (42) Olsen, J. M.; Aidas, K.; Kongsted, J. Excited States in Solution through Polarizable Embedding. *J. Chem. Theory Comput.* **2010**, *6*, 3721–3734.
- (43) Guido, C. A.; Jacquemin, D.; Adamo, C.; Mennucci, B. Electronic Excitations in Solution: The Interplay between State Specific Approaches and a Time-Dependent Density Functional Theory Description. *J. Chem. Theory Comput.* **2015**, *11*, 5782–5790.
- (44) Ren, S.; Lipparini, F.; Mennucci, B.; Caricato, M. Coupled Cluster Theory with Induced Dipole Polarizable Embedding for Ground and Excited States. *J. Chem. Theory Comput.* **2019**, *15*, 4485–4496.
- (45) Lunkenheimer, B.; Köhn, A. Solvent Effects on Electronically Excited States Using the Conductor-Like Screening Model and the

- Second-Order Correlated Method Adc(2). J. Chem. Theory Comput. 2013, 9, 977-994.
- (46) Mewes, J.-M.; You, Z.-Q.; Wormit, M.; Kriesche, T.; Herbert, J. M.; Dreuw, A. Experimental Benchmark Data and Systematic Evaluation of Two a Posteriori, Polarizable-Continuum Corrections for Vertical Excitation Energies in Solution. *J. Phys. Chem. A* **2015**, *119*, 5446–5464.
- (47) Gao, J.; Byun, K. Solvent Effects on the $N\pi^*$ Transition of Pyrimidine in Aqueous Solution. *Theor. Chem. Acc.* **1997**, *96*, 151–156. (48) Lin; Gao, J. Solvatochromic Shifts of the $N \to \Pi^*$ Transition of Acetone from Steam Vapor to Ambient Aqueous Solution: A Combined Configuration Interaction QM/MM Simulation Study Incorporating Solvent Polarization. *J. Chem. Theory Comput.* **2007**, *3*, 1484–1493.
- (49) Kosenkov, D.; Slipchenko, L. V. Solvent Effects on the Electronic Transitions of P-Nitroaniline: A Qm/Efp Study. *J. Phys. Chem. A* **2011**, *115*, 392–401.
- (50) Ghosh, D.; Isayev, O.; Slipchenko, L. V.; Krylov, A. I. Effect of Solvation on the Vertical Ionization Energy of Thymine: From Microhydration to Bulk. *J. Phys. Chem. A* **2011**, *115*, 6028–6038.
- (51) Flick, J. C.; Kosenkov, D.; Hohenstein, E. G.; Sherrill, C. D.; Slipchenko, L. V. Accurate Prediction of Noncovalent Interaction Energies with the Effective Fragment Potential Method: Comparison of Energy Components to Symmetry-Adapted Perturbation Theory for the S22 Test Set. *J. Chem. Theory Comput.* **2012**, *8*, 2835–2843.
- (52) Slipchenko, L. V.; Gordon, M. S. Damping Functions in the Effective Fragment Potential Method. *Mol. Phys.* **2009**, *107*, 999–1016.
- (53) Jorgensen, W. L.; Tirado-Rives, J. Potential Energy Functions for Atomic-Level Simulations of Water and Organic and Biomolecular Systems. *Proc. Natl. Acad. Sci. U.S.A.* **2005**, *102*, 6665–6670.
- (54) Dodda, L. S.; Cabeza de Vaca, I.; Tirado-Rives, J.; Jorgensen, W. L. Ligpargen Web Server: An Automatic Opls-Aa Parameter Generator for Organic Ligands. *Nucleic Acids Res.* **2017**, *45*, W331–W336.
- (55) Dodda, L. S.; Vilseck, J. Z.; Tirado-Rives, J.; Jorgensen, W. L. 1.14*Cm1a-Lbcc: Localized Bond-Charge Corrected Cm1a Charges for Condensed-Phase Simulations. *J. Phys. Chem. B* **2017**, *121*, 3864–3870
- (56) Abraham, M. J.; Murtola, T.; Schulz, R.; Páll, S.; Smith, J. C.; Hess, B.; Lindahl, E. Gromacs: High Performance Molecular Simulations through Multi-Level Parallelism from Laptops to Supercomputers. *SoftwareX* **2015**, *1*–2, 19–25.
- (57) Schmidt, M. W.; Baldridge, K. K.; Boatz, J. A.; Elbert, S. T.; Gordon, M. S.; Jensen, J. H.; Koseki, S.; Matsunaga, N.; Nguyen, K. A.; Su, S.; et al. General Atomic and Molecular Electronic Structure System. *J. Comput. Chem.* **1993**, *14*, 1347–1363.
- (58) Barca, G. M.; Bertoni, C.; Carrington, L.; Datta, D.; De Silva, N.; Deustua, J. E.; Fedorov, D. G.; Gour, J. R.; Gunina, A. O.; Guidez, E.; et al. Recent Developments in the General Atomic and Molecular Electronic Structure System. *J. Chem. Phys.* **2020**, *152*, 154102.
- (59) Chai, J.-D.; Head-Gordon, M. Systematic Optimization of Long-Range Corrected Hybrid Density Functionals. *J. Chem. Phys.* **2008**, *128*, 084106.
- (60) Chai, J.-D.; Head-Gordon, M. Long-Range Corrected Hybrid Density Functionals with Damped Atom-Atom Dispersion Corrections. *Phys. Chem. Chem. Phys.* **2008**, *10*, 6615–6620.
- (61) Epifanovsky, E.; Gilbert, A. T. B.; Feng, X.; Lee, J.; Mao, Y.; Mardirossian, N.; Pokhilko, P.; White, A. F.; Coons, M. P.; Dempwolff, A. L.; et al. Software for the Frontiers of Quantum Chemistry: An Overview of Developments in the Q-Chem 5 Package. *J. Chem. Phys.* **2021**, *155*, 084801.
- (62) Kaliman, I. A.; Slipchenko, L. V. Libefp: A New Parallel Implementation of the Effective Fragment Potential Method as a Portable Software Library. *J. Chem. Theory Comput.* **2013**, 34, 2284–2292.
- (63) Kaliman, I. A.; Slipchenko, L. V. Hybrid Mpi/Openmp Parallelization of the Effective Fragment Potential Method in the Libefp Software Library. J. Chem. Theory Comput. 2015, 36, 129–135.

- (64) Parrish, R. M.; Sitkoff, D. F.; Cheney, D. L.; Sherrill, C. D. The Surprising Importance of Peptide Bond Contacts in Drug-Protein Interactions. *Chem.—Eur. J.* **2017**, *23*, 7887–7890.
- (65) Olsen, J. M.; Aidas, K.; Mikkelsen, K. V.; Kongsted, J. Solvatochromic Shifts in Uracil: A Combined Md-Qm/Mm Study. *J. Chem. Theory Comput.* **2010**, *6*, 249–256.
- (66) Marian, C.; Schneider, F.; Kleinschmidt, M.; Tatchen, J. Electronic Excitation and Singlet-Triplet Coupling in Uracil Tautomers and Uracil-Water Complexes: A Quantum Chemical Investigation. *Eur. Phys. J. D* **2002**, *20*, 357–367.
- (67) Epifanovsky, E.; Kowalski, K.; Fan, P.-D.; Valiev, M.; Matsika, S.; Krylov, A. I. On the Electronically Excited States of Uracil. *J. Phys. Chem. A* **2008**, *112*, 9983–9992.
- (68) Kistler, K. A.; Matsika, S. Solvatochromic Shifts of Uracil and Cytosine Using a Combined Multireference Configuration Interaction/Molecular Dynamics Approach and the Fragment Molecular Orbital Method. *J. Phys. Chem. A* **2009**, *113*, 12396–12403.
- (69) Fu, F.; Liao, K.; Ma, J.; Cheng, Z.; Zheng, D.; Gao, L.; Liu, C.; Li, S.; Li, W. How Intermolecular Interactions Influence Electronic Absorption Spectra: Insights from the Molecular Packing of Uracil in Condensed Phases. *Phys. Chem. Chem. Phys.* **2019**, *21*, 4072–4081.
- (70) Mukherjee, M.; Tripathi, D.; Brehm, M.; Riplinger, C.; Dutta, A. K. Efficient Eom-Cc-Based Protocol for the Calculation of Electron Affinity of Solvated Nucleobases: Uracil as a Case Study. *J. Chem. Theory Comput.* **2021**, *17*, 105–116.
- (71) Voet, D.; Gratzer, W.; Cox, R.; Doty, P. Absorption Spectra of Nucleotides, Polynucleotides, and Nucleic Acids in the Far Ultraviolet. *Biopolymers* **1963**, *1*, 193–208.
- (72) Clark, L. B.; Peschel, G. G.; Tinoco, I., Jr. Vapor Spectra and Heats of Vaporization of Some Purine and Pyrimidine Bases 1. *J. Phys. Chem.* **1965**, *69*, 3615–3618.
- (73) Daniels, M.; Hauswirth, W. Fluorescence of the Purine and Pyrimidine Bases of the Nucleic Acids in Neutral Aqueous Solution at 300°K. *Science* **1971**, *171*, 675–677.
- (74) Du, H.; Fuh, R.-C. A.; Li, J.; Corkan, L. A.; Lindsey, J. S. Photochemcad‡: A Computer-Aided Design and Research Tool in Photochemistry. *Photochem. Photobiol.* **1998**, *68*, 141–142.